Scripta Materialia 234 (2023) 115540

Contents lists available at ScienceDirect

Scripta Materialia

journal homepage: www.journals.elsevier.com/scripta-materialia

Direct evidence of the shockley tetragonal L1' phase in a bulk Fe-Pd alloy

A. Savovici *, W.A. Soffa, J.A. Floro

Department of Materials Science and Engineering, University of Virginia, 395 McCormick Road, Charlottesville, VA 22904, USA

ARTICLE INFO

Keywords:
Phase transformations
Hard magnetic materials
Order/Disorder
L10

ABSTRACT

Direct evidence is provided for the existence of the tetragonal L1' phase, first predicted by Shockley in 1938, in bulk Fe - 62 at% Pd alloys aged at 525 °C. L1' existence as the dominant phase is supported by quantitative x-ray diffraction analysis. This is combined with transmission electron microscopy of the polytwinned microstructure, examining the diffracted intensities in specific superlattice reflections where the complete extinction in $L1_0$ is relaxed in L1'. Ordering to L1' appears to occur directly from the A1 parent phase at 525 ºC, while aging at 650 ºC only produces $L1_0$. The possibility of L1' ordering may have consequences for the ferromagnetic properties of classic and important binary alloy systems where $L1_0$ is the assumed equilibrium phase.

Metallic alloys that chemically order to the $L1_0$ crystal structure have been intensively studied in the context of the theory of phase transformations, and due to their potential as hard ferromagnets, where specific alloys can exhibit high uniaxial magnetocrystalline anisotropy (K_u) and high coercivity (H_c). The A1→$L1_0$ transformation is among the most heavily-investigated disorder-order transformations, yielding key insights into the role of anisotropic transformation strain on spatial self-organization of the product phase. This, for example, leads to the well-known *polytwin* structure [1,2] that will be discussed in more detail below. In addition, many binary alloys that order to $L1_0$ near the 1:1 composition, also order to $L1_2$ near 1:3 and/or 3:1 compositions. The two ordered phases are connected by a eutectoid transformation, A1→$L1_0$+$L1_2$. The $L1_0$+$L1_2$ coexistence regions in alloys such as Fe-Pt, Co-Pt and Fe-Pd are very poorly explored, but are of significant interest in the context of exchange-coupled ferromagnetism, since $H_c(L1_0) >> H_c$ ($L1_2$). Again, the anisotropic cubic→tetragonal transformation strain can lead to fascinating forms of spatial self-organization. This includes the *nanochessboard* structure, discovered by Leroux, et al., in Co-Pt alloys [3]. We recently reported on exchange-coupled ferromagnetic behavior of Co-Pt chessboards [4–8].

Interest in $L1_0$ ferromagnetism recently received renewed impetus with the discovery of a facile casting methodology to achieve $L1_0$ ordering in bulk Fe-Ni alloys with the addition of P [9]. This advance could lead to the fabrication of high-performance permanent magnets without precious or rare-earth metallic components. In the course of investigating phase formation and microstructure evolution in bulk Fe-Pd alloys with compositions near the A1→$L1_0$+$L1_2$ eutectoid, we have found strong evidence for the equilibrium existence of the L1' phase. This phase was first predicted by Shockley in 1938, [10] but to our knowledge, has only been observed once, in Fe-Pd thin films, [11] and even there, indirectly. The L1' phase is most likely to form when the $L1_0$ composition deviates significantly from the equimolar one, which is generally the case when working within or near the $L1_0$+$L1_2$ coexistence regions. Indeed, the L1' can be visualized as a hybrid form of these two phases. Note that the use of off-stoichiometric compositions in $L1_0$ is a requirement in Fe-Pt alloys in order to achieve hard ferromagnetic behavior in bulk [12,13]. Off-stoichiometric compositions also occurred in bulk Fe-Ni $L1_0$ that was formed by casting with P additions [9].

Beyond just verifying the existence of the L1' phase, it is important to understand its thermodynamic origins and the evolution of ordering, as well as the resulting defect structure. This has fundamental importance to our understanding of phase equilibria and disorder-order / order-order theory. It also likely impacts the ferromagnetism. The structure of L1' will modify the ferromagnetic properties relative to $L1_0$, including the magnetocrystalline anisotropy and saturation magnetization, while potentially proliferating antiphase boundaries that can promote domain wall pinning. Here we provide the key evidence for L1' in the Fe-Pd system, obtained from x-ray diffraction (XRD) and transmission electron microscopy (TEM).

$L1_0$ and L1' are both P4/mmm but differ in the arrangement of off-stoichiometric excess atoms on the tetragonal lattice (Fig. 1). When there is excess concentration relative to equimolar, $A_{1+\delta}B_{1-\delta}$, $L1_0$ ordering distributes the excess A atoms evenly across *all* B-sites, while L1' further orders by preferentially locating the excess A atoms solely on the (½, ½, 0) site on the (001) planes. Steiner, et al. [11], rigorously defined a model with two order parameters to capture the different

* Corresponding author.
E-mail address: as5fj@virginia.edu (A. Savovici).

https://doi.org/10.1016/j.scriptamat.2023.115540
Received 20 December 2022; Received in revised form 2 May 2023; Accepted 6 May 2023
Available online 12 May 2023

Table 1
Structure factor calculations for important low-angle superlattice reflections in L1'. Here M is the multiplicity factor, while |F| is the structure factor value for Cu-Kα x-rays and 300 kV electrons, as indicated.

hkl	F_{hkl}	*M (XRD)*	F_{hkl} *(Cu − Kα)*	F_{hkl} *(300 kV e⁻)*
100	$\mathbf{f_{Fe} - f_{FePd}}$	4	9.09	0.71
001	$\mathbf{f_{Fe} + f_{FePd} - 2f_{Pd}}$	2	28.68	2.27
110	$\mathbf{f_{Fe} - f_{FePd}}$	4	26.72	2.50
101	$\mathbf{f_{Fe} + f_{FePd} - 2f_{Pd}}$	8	8.41	0.79

Table 2
This table shows ratios of measured / calculated intensity ratios for the hallmark L1′ superlattice reflections, and a general superlattice/fundamental ordering parameter for $L1_0$ & L1′.

Crystal Structure	$\frac{I_{\{100\}}}{I_{(001)}}$	$\frac{I_{\{101\}}}{I_{(110)}}$	$\frac{I_{(001)}}{I_{(002)}}$
	Measured/Maximum	*Measured/Maximum*	*Measured/Maximum*
$L1'$	0.854	0.731	0.825
$L1_0$	–	–	0.945

degrees of order possible within the L1'crystal structure. In our work, quantitative x-ray diffraction analysis, combined with microstructure imaging in transmission electron microscopy, provides direct and powerful evidence for L1' as a primary phase in bulk Fe-Pd alloys.

An Fe-Pd boule was arc-melted from 99.99% Fe and 99.9% Pd chunks in an argon ambient environment, with a Pd content of 62 ± 0.5 at% Pd, determined after melting using inductively coupled optical emission spectroscopy (ICP-OES). Subsequent thermomechanical treatments yielded samples of ~200um thickness, achieved by repeated cold-rolling and recrystallization with 24hr homogenization treatments at 1000 °C. All samples were annealed in tube furnaces while encapsulated in argon-backfilled fused quartz ampules, then water quenched. Structural analysis was performed on a Panalytical Empyrean X-ray diffractometer (XRD) with Cu-Kα1 radiation and parallel beam θ–2θ geometry after a polishing sequence down to 3 μm diamond slurry was carried out. Quantitative analysis of XRD peak intensity ratios accounted for multiplicity, Lorentz-polarization factors, atomic scattering factors, and Debye–Waller thermal factors [11]. Microstructure was characterized using transmission electron microscopy (TEM) performed on a ThermoFisher Titan operating at 300 kV. Thin foils were prepared in a Fischione twin-jet electropolisher using an electrolyte of 82% acetic acid, 9% perchloric acid, and 9% ethanol (by volume) at 0 °C and approximately 30 Vs.

Two samples of the alloy were first solutionized in the A1 phase at 850ºC, quenched, then aged for 10 days, one sample at 650 °C and the other at 525 °C. Fig. 2 shows XRD patterns for each sample. When aged at 650 °C, a diffraction pattern results that is fully consistent with single-phase $L1_0$ structure, see Fig. 2. The lattice parameters determined from {200} are $a_{L1_0} = 3.853$ Å, $c_{L1_0} = 3.706$ Å . However, when aged at 525ºC, Fig. 2 shows that new peaks emerge in the vicinity of the $L1_0$ (001) and (110) superlattice reflections, while the (002) reflection moves to lower Bragg angle. The new peaks are consistent with L1', where, unlike $L1_0$, both {100} and (001) reflections are allowed, as are {101} and (110). The lattice parameters for L1' are $a_{L1'} = 3.853$ Å, $c_{L1'} = 3.747$ Å.

Quantitative analysis of these L1'-only reflections is afforded by structure factor calculations shown in Table 1. In column 2, $\mathbf{f_{Fe}}$ represents the atomic scattering factor for (0,0,0) site occupied by Fe solely, $\mathbf{f_{FePd}}$ is the (1/2,1/2,0) site occupied by a combination of Fe & Pd (in our particular alloy, $\mathbf{f_{FePd}} = 0.48\,\mathbf{f_{Pd}} + 0.52\,\mathbf{f_{Fe}}$), and $\mathbf{f_{Pd}}$ sites correspond to the (1/2,0,1/2) and (0,1/2,1/2) sites which (at our composition) are occupied solely by Pd. Placement of Pd solely on this site is an ansatz we make consistent with Shockley's original calculations for completely-

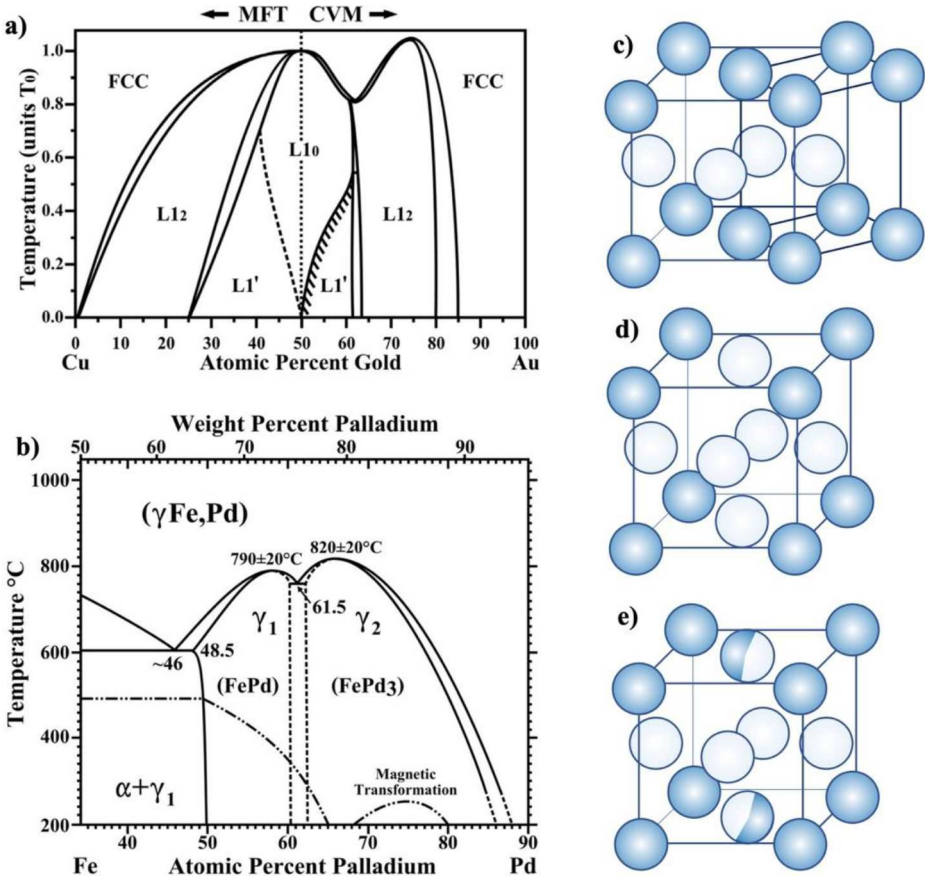

Fig. 1. a) Schematic Cu-Au phase diagram [11] displaying Mean Field Theory (left) and Cluster Variation Method (right) calculations showing stability of the low-temperature tetragonal L1′ phase. b) A portion of the Fe-Pd phase diagram showing the high-temperature A1 phase, and the $L1_0$ + $L1_2$ two-phase coexistence region explored in this work (taken from [14]) c) In these figures darker atoms are iron (Fe), while light atoms are palladium (Pd). The stoichiometric FePd $L1_0$ unit cell is shown in c) with a primitive unit cell inlay, while in d) the ordered cubic $FePd_3$ $L1_2$ structure is shown. In e) a prototypic L1' crystal structure with secondary (001) plane ordering is displayed at an arbitrary composition. In the Shockley L1' structure, off-stoichiometric excess concentration of one component (here, the lighter colored element) is accommodated solely on the basal plane center site as shown.

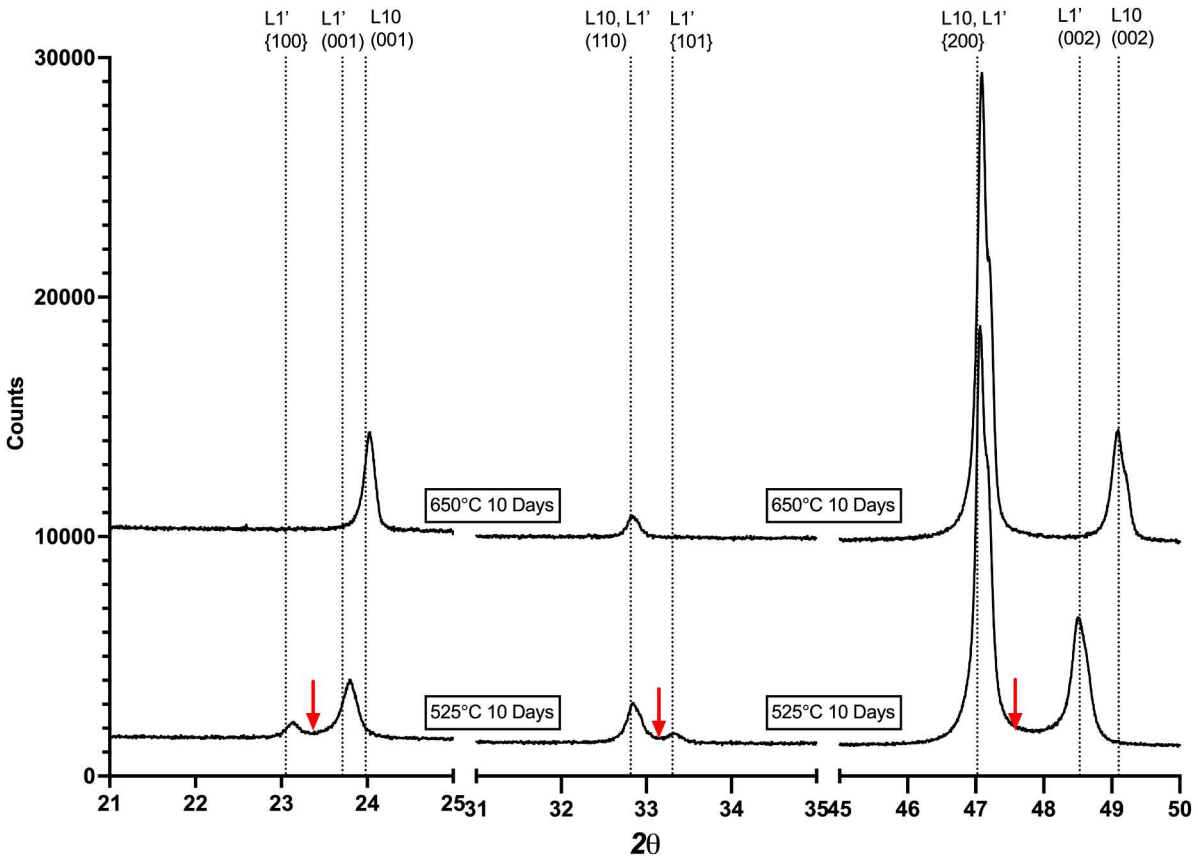

Fig. 2. X-ray diffractograms of Fe – 62 at% Pd samples aged for 10D at 650 °C and 525 °C. Select 2θ regions are displayed to highlight structural differences between the high temperature phase ($L1_0$) and low temp phase (L1'). All vertical dashed lines are based on lattice parameters determined from the {200} and (002) peaks of the L10 phase at 650 °C. The red arrows indicate the expected locations of superlattice & fundamental reflection for the $L1_2$ phase.

ordered material, allowing us to analyze ordering using a single order parameter, and should be reasonable when the degree of order is high, as it is here. It is also fully motivated by and consistent with our fundamental observation of new Bragg peaks splitting off the $L1_0$ superlattice reflections.

If the structure is ordered as $L1_0$ instead, such that excess Pd is distributed evenly across all the Fe sites, then $F_{100} = F_{101} = f_{FePd} - f_{FePd} = 0$. The absolute structure factor values in column 4 are computed using atomic scattering constants for comparison against XRD results, while in column 5 the electron scattering constants are used, to support TEM analysis below. Ratios of intensities from our structure factor calculations were compared against values generated from an on-composition Fe-Pd L1' crystal in the Vesta package, and obtained full quantitative agreement.

Further confirmation of L1' is afforded by quantitative analysis of the peak intensity ratios. An order parameter is calculated from the diffraction spectra shown as the of ratio of superlattice/fundamental reflections, namely $\frac{I_{(001)}}{I_{(002)}}$. This measured value is then compared against theoretical maximums generated from structure factor calculations (see Table 2). While theoretical order parameters employing the Steiner, et al. approach [11] or a Bragg-Williams approach [15] are possible, for these calculations we are calculating values using the chemical occupancy on a pseudo-cubic, face-centered lattice with indices tied to the original A1 parent phase. Table 2 also lists measured intensity ratios of L1'-only reflections normalized by theoretical ratios, and shows that all measured intensity ratios are similar to, but somewhat smaller than, the predicted values – importantly, the measured values never exceed the theoretical values, which would indicate problems with phase identification. The reduced values of the observed intensity ratios are readily explained by incomplete ordering at 525°C due to sluggish diffusion. The order parameter for L1' is 82% of the maximum value possible at this composition. For the $L1_0$ phase obtained at 650 °C, where kinetics are more rapid, the order parameter is within 94% of the maximum value.

L1' also exhibits a marked reduction of tetragonality vis-à-vis $L1_0$, corresponding to an increase in the c/a ratio (when indexed to the conventional, pseudo-cubic unit cell) that owes to the hybrid $L1_0/L1_2$ nature of the L1' phase. Since excess off-stoichiometric Pd atoms in the tetragonal crystal are placed on a site that, if completely populated by Pd, would result in $FePd_3$ $L1_2$ structure, it seems likely that the lattice should adjust to reduce the tetragonal distortion [11]. Our results (Fig. 2) support this hypothesis: $c/a_{L10} \approx 0.961$, while $c/a_{L1'} \approx 0.972$.

An alternative explanation for the additional XRD peaks shown for L1' (i.e. {100} & {101}) in Fig. 2 would be that the $L1_2$ phase is forming. Indeed, we have observed coexistence of $L1_0 + L1_2$ as predicted by the equilibrium phase diagram for Fe-Pd, at slightly more Pd-rich compositions and elevated temperatures (650 °C). Those results allow us to identify the locations of $L1_2$ peaks, which are indicated by red arrows on Fig. 2. The new ordering peaks clearly do not lie at these positions; as such, we reject coexistence of $L1_0$+$L1_2$ as an explanation for the XRD spectra.

Microstructure analysis lends further insights into the phase formation. TEM imaging of the sample aged at 525°C, see Fig. 3, reveals polytwin microstructure – parallel lamellae with alternating orientation of the tetragonal c-axis along two of the three original cube directions. The twin lamellae are separated by {110} planes (sometimes referred to as orientation domain walls, or ODWs) having invariant plane strain. This microstructure is a frequent outcome of the A1→$L1_0$ transformation, as it minimizes the cubic→tetragonal transformation strain during

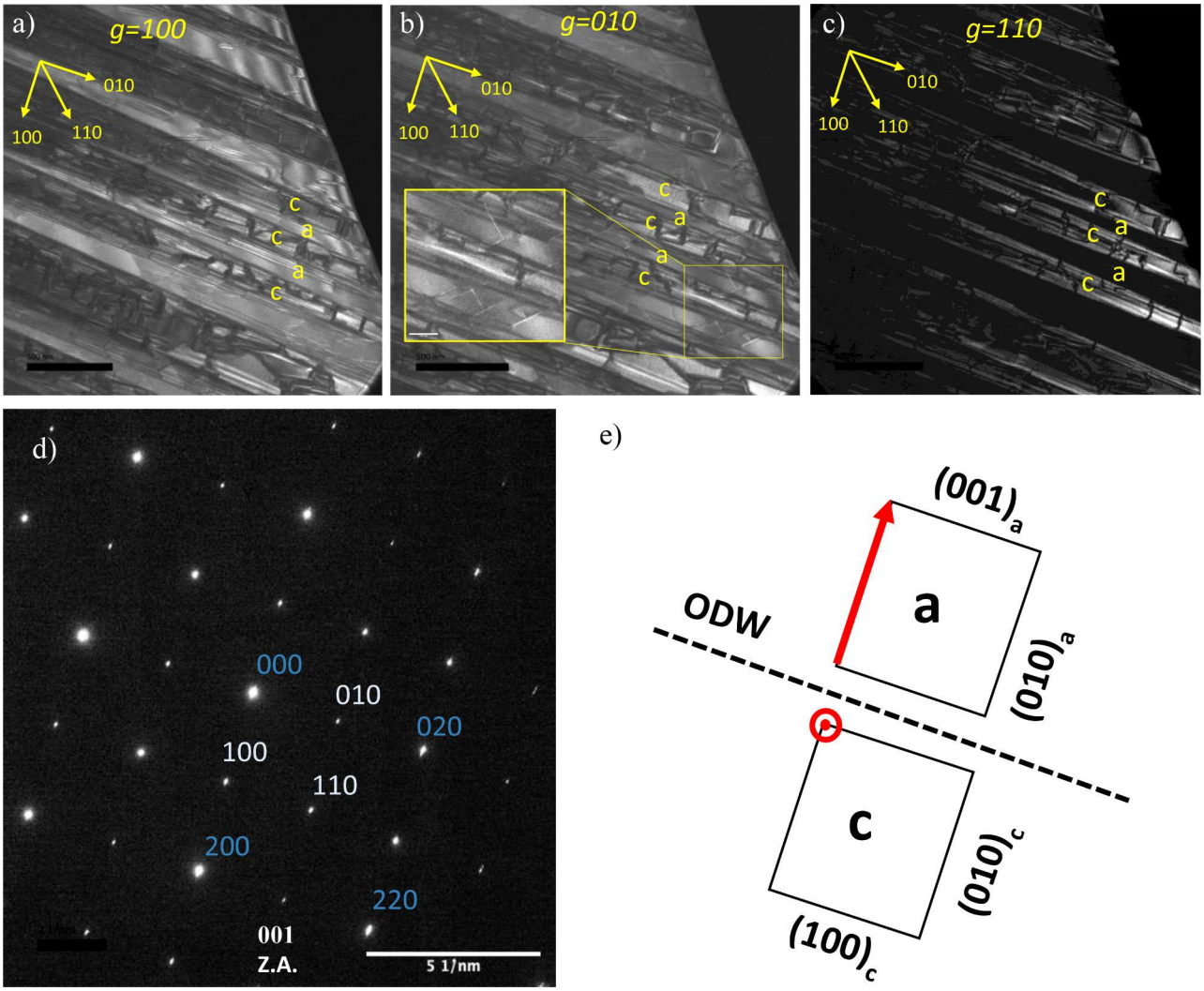

Fig. 3. TEM highlighting the L1' polytwin microstructure, where c and a orientation variants are separated by (101) orientation domain boundaries. (a), g = 100 dark field produces more intensity in the a-variant since the $(001)_a$ structure factor is 3x larger than the $(100)_c$ of the c-variant. Similarly, in (b) g = 010 dark field produces more uniform intensity, while in (c) g = 110 dark field strongly lights up the c-variant.(d) The SADP of this region. (e) Schematic of the a & c orientation variant unit cells, where the c-axes in each are shown in red.

ordering, and would also be expected for A1→L1'.

Fig. 3 shows dark-field micrographs captured from an L1' polytwin region, with a [001] zone axis. Herein, all planes and indices are referred to the original A1 matrix unless otherwise noted. Fig. 3d shows the selected area electron diffraction pattern (SADP). The ODWs in Fig. 3 are along (101) planes, tilted at 45° to the image plane. See Fig. 3e for the arrangement of the variant unit cells. In a prototypical $L1_0$ polytwin microstructure imaged under dark-field conditions, the orientations of the domain variants may be individually identified using specific *g*-vectors (*g* is the reciprocal lattice vector satisfying Bragg diffraction) that isolate reflections from a single variant. However, in L1', superlattice reflections not allowed in $L1_0$ will create contrast in an otherwise 'dark', or non-contributing $L1_0$ variant. For example, in Fig. 3a, the $g = 100$ condition aligns perfectly with the strong $(001)_a$ superlattice reflection of the a-variant. In addition, this *g*-vector imaging condition will have intensity contributions from the c-variant $(100)_c$ reflection, as the reciprocal lattice points partially overlap. The contribution from the two distinct planes of the different orientation variants creates the noticeable intensity variation between the white (*c*-variants) and gray (*a*-variants) regions that constitute the L1' polytwin microstructure. This is consistent with Table 1, column 5, which indicates that the diffracted intensity from $(001)_a$ is about 3x stronger than that from $(100)_c$. Fig. 3b shows the $g = 010$ dark field imaging condition, where a more uniform gray contrast is seen across both *a* and *c*-variants. This is because the intensity found for this condition (in both variants) is created by the weakly diffracting L1'-only superlattice reflection, (010). Similar results are obtained in Fig. 3c for the $g = 110$ condition from the strong $(110)_c$ vs. weak $(011)_a$ reflections (while the a-reflections appear black in Fig. 3c, this is the result of overall underexposure of the entire image). Again, this is consistent with structure factor calculations in Table 1 for 300 kV electrons.

The SADP of Fig. 3d shows three superlattice reflections, 100, 010, and 110. As demonstrated in Fig. 3, dark-field imaging using these g-vectors lights up extended regions of the micrograph, so none of these reflections arises solely from a minority phase. For $L1_0$, one block of polytwin *c*-domains in a mature structure can only contain *two c*-axis orientation variants; in which case all three superlattice reflections will not be present simultaneously in $L1_0$. However, for L1', restrictions on missing reflections are greatly reduced (Table 1), and mature L1' polytwin blocks are expected to produce the SADP shown in Fig. 3d.

The inset of Fig. 3b also shows the presence of faceted antiphase boundaries (APBs). Their extended morphology is further highlighted in

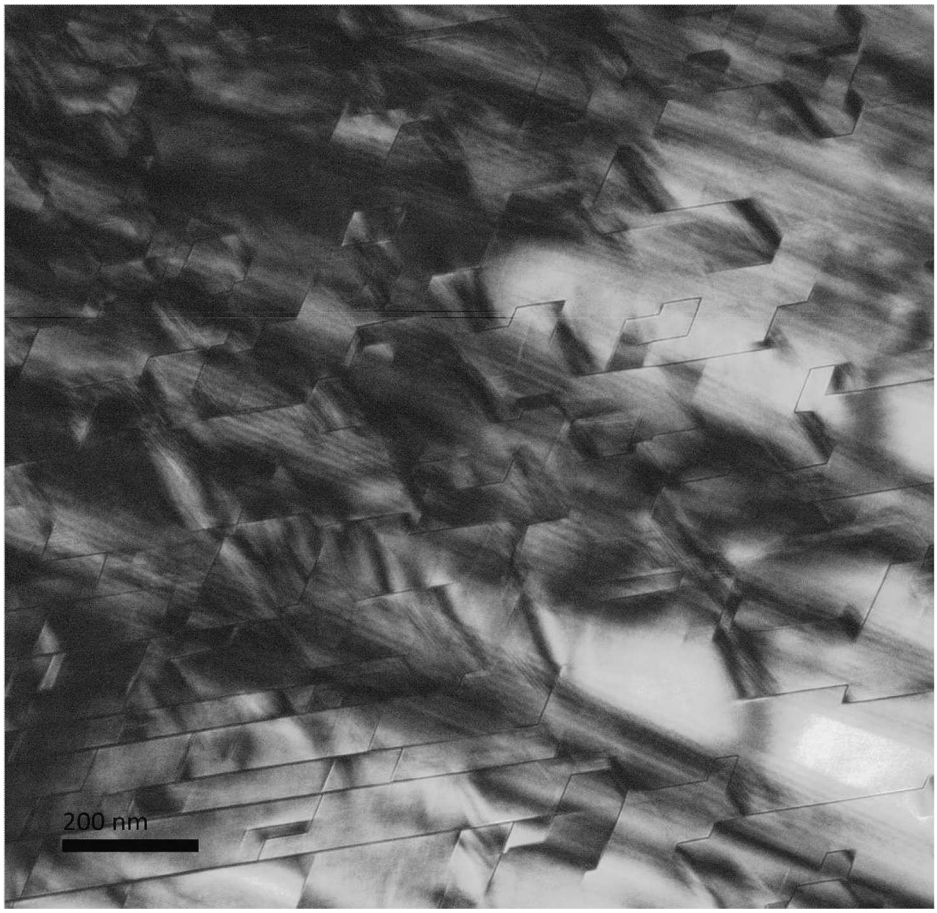

Fig. 4. $g = 1\bar{1}0$ dark field micrograph along a [111] zone axis, showing the intricate mosaic of polygonised APBs within the samples aged at 525 °C.

Fig. 4, along a [111] zone axis. This is a different region of the sample than Fig. 3, and while similar, it may represent a more evolved state of the microstructure. These APBs have polygonized along a subset of {110} planes and dark-field imaging in the inset of Fig 3b (also for the APBs of Fig. 4, not shown here) indicates that the APBs are decorated by plates a few nm thick of another phase or orientation variant.

These APBs bear visual resemblance to "platelets" observed in Co-Pt alloys that were aged at high temperatures in the $L1_0$-$L1_2$ coexistence regions, [16–18] where fully-ordered $L1_2$ decomposed towards equilibrium $L1_2 \rightarrow L1_2 + L1_0$, and $L1_0$ nucleation occurred on APBs. Hence APBs in that system became pairs of interphase boundaries (IPBs), using the terminology of Kikuchi and Cahn [19]. Crucially, however, the platelets in [17] do not lie along low-index crystallographic planes, but instead orient to minimize elastic and surface energy. In this sense, the APBs in Fig. 3 are quite different, as they rigorously facet on {110}. Generally, in $L1_0$ and $L1_2$ ordered phases, {100} planes are held to be the low energy APB orientation. Preliminary extinction analysis of the APBs imaging with different g-vectors suggests the presence of ½[110] antiphase translation vectors allowed in L1' but not in $L1_0$. This is beyond the scope of this paper, and the structure and origins of the unusually-polygonized APBs seen here are also still being investigated.

In conclusion, we present *direct* evidence from x-ray diffraction and transmission electron microscopy for the long-theorized L1' phase, and the first evidence of any kind for existence as the primary phase in a bulk material. The phase has formed in Fe-Pd alloys with compositions in or near the $L1_0$+$L1_2$ coexistence region. In these experiments, L1' formed from a metastable A1 precursor during aging at 525ºC. While we cannot rule out a two-step transformation A1→L10→L1', there is no inherent reason that A1→L1' cannot occur directly, likely by nucleation + growth of the tetragonal phase within the matrix. A unique polygonization of APBs was also observed in the system, organizing along {110} planes and most likely forming IPBs. As L1' will affect magnetic properties, it is important to examine whether it occurs in other $L1_0$-forming systems when there is significant deviation from equimolar stoichiometry.

Declaration of Competing Interest

The authors declare that they have no known competing financial interests or personal relationships that could have appeared to influence the work reported in this paper.

Acknowledgment

We acknowledge Wade Jensen for arc-melting the Fe-Pd. We thank Helge Heinrich for his support in TEM imaging. Support by the National Science Foundation under Grant DMR-1709914 is gratefully acknowledged.

References

[1] T. Klemmer, D. Hoydick, H. Okumura, B. Zhang, W.A. Soffa, Magnetic hardening and coercivity mechanisms in $L1_0$ ordered FePd ferromagnets, Scripta Metall. Mater. 33 (10–11) (1995) 1793–1805, https://doi.org/10.1016/0956-716x(95)00413-p.

[2] D.E. Laughlin, K. Srinivasan, M. Tanase, L. Wang, Crystallographic aspects of $L1_0$ magnetic materials, Scripta Mater. 53 (4) (2005) 383–388, https://doi.org/10.1016/j.scriptamat.2005.04.039.

[3] C. Leroux, A. Loiseau, D. Broddin, G. Vantendeloo, Electron microscopy study of the coherent two-phase mixtures L10+ L12, in Co–Pt alloys, Philosoph. Mag. B 64 (1) (1991) 57–82, https://doi.org/10.1080/13642819108207603.

[4] J.A. Floro, E.P. Vetter, P. Ghatwai, L.D. Geng, Y.M. Jin, W.A. Soffa, Hierarchical structure and the origins of coercivity in exchange-coupled Co-Pt nanochessboards, J. Magn. Mater. 487 (May) (2019), https://doi.org/10.1016/j.jmmm.2019.165313.
[5] E.P. Vetter, L. Geng, P. Ghatwai, et al., Lengthscale effects on exchange coupling in Co-Pt L10 + L12 nanochessboards, APL Mater. 4 (9) (2016), 096103, https://doi.org/10.1063/1.4962187.
[6] I. Kashyap, E.P. Vetter, J.A. Floro, M. De Graef, Lorentz TEM study of the magnetic microstructure in near-eutectoid Co-Pt alloys, J. Magn. Magn. Mater. 479 (2019) 204–211, https://doi.org/10.1016/j.jmmm.2019.02.036.
[7] E. Vetter, P. Ghatwai, W. Soffa, J. Floro, Evolution of First-Order Reversal Curves During Self-Assembly of the Co40.2Pt59.8 Nano-Chessboard Structure, IEEE Magn. Lett. 6 (2015) 1–4, https://doi.org/10.1109/lmag.2015.2480386.
[8] L.D. Geng, W.A. Soffa, J.A. Floro, Y.M. Jin, Exchange coupling effects in Co-Pt nanochessboards, J. Appl. Phys. 123 (9) (2018), 093901, https://doi.org/10.1063/1.5019841.
[9] Y.P. Ivanov, B. Sarac, S.V. Ketov, J. Eckert, A.L. Greer, Direct formation of hard-magnetic tetrataenite in bulk alloy castings, Adv. Sci. (2022), 2204315, https://doi.org/10.1002/advs.202204315.
[10] W. Shockley, Theory of order for the copper gold alloy system, J. Chem. Phys. 6 (3) (1938) 130–144, https://doi.org/10.1063/1.1750214.
[11] M.A. Steiner, R.B. Comes, J.A. Floro, W.A. Soffa, J.M. Fitz-Gerald, L1′ ordering: evidence of $L1_0$-$L1_2$ hybridization in strained $Fe_{38.5}Pd_{61.5}$ epitaxial films, Acta Mater. 85 (2015) 261–269, https://doi.org/10.1016/j.actamat.2014.11.036.
[12] Y. Tanaka, N. Kimura, K. Hono, K. Yasuda, T. Sakurai, Microstructures and magnetic properties of Fe-Pt permanent magnets, J. Magn. Magn. Mater. 170 (3) (1997) 289–297, https://doi.org/10.1016/s0304-8853(97)00019-x.
[13] T. Goto, H. Utsugi, K. Watanabe, Effect of atomic order-disorder on 57Fe hyperfine structure in Fe64Pt36 alloy, J. Alloy. Compd. 204 (1–2) (1994) 173–178, https://doi.org/10.1016/0925-8388(94)90087-6.
[14] M.A. Steiner, R.B. Comes, J.A. Floro, W.A. Soffa, J.M. Fitz-Gerald, V. S. Smentkowski, Strain induced microstructural and ordering behaviors of epitaxial Fe38.5Pd61.5films grown by pulsed laser deposition, J. Vac. Sci. Technol. A: Vac. Surface. Film. 31 (5) (2013), 050824, https://doi.org/10.1116/1.4819376.
[15] W.L. Bragg, E.J. Williams, The effect of thermal agitation on atomic arrangement in alloys, Proc. R. Soc. Lond. A 145 (855) (1934) 699–730, https://doi.org/10.1098/rspa.1934.0132.
[16] C. Leroux, A. Loiseau, M.C. Cadeville, F. Ducastelle, Wetting of Antiphase Boundaries by the Disordered Phase in CoPt 3, Europhys. Lett. 12 (2) (1990) 155–160, https://doi.org/10.1209/0295-5075/12/2/011.
[17] Y. Le Bouar, A Loiseau, Strain-induced microstructure development due to a wetting phenomenon in the Co–Pt system, Acta Mater. 49 (14) (2001) 2679–2690, https://doi.org/10.1016/s1359-6454(01)00173-2.
[18] Y. Le Bouar, A.G Khachaturyan, Mechanism and modeling of saw-tooth structure formation in the L12–L10 two-phase system, Acta Mater. 48 (8) (2000) 1705–1717, https://doi.org/10.1016/s1359-6454(00)00017-3.
[19] R. Kikuchi, J.W. Cahn, Theory of interphase and antiphase boundaries in F.C.C. alloys, Acta Metall. 27 (8) (1979) 1337–1353, https://doi.org/10.1016/0001-6160(79)90203-7.